Lasers in Surgery and Medicine 50:1034–1039 (2018)

Smartphone Imaging of Subcutaneous Veins

William Lewis and Walfre Franco
Wellman Center for Photomedicine, Massachusetts General Hospital, Boston, Massachusett and Department of Dermatology, Harvard Medical School, Boston, Massachusetts

Objective: The identification of veins by medical personnel is a critical skill that is necessary to draw blood or administer intravenous fluids and medications. Because a normal consumer camera can act as a multispectral imaging apparatus, operating with three broadband detectors, we hypothesized that a standard smartphone camera might be employed for enhanced visualization of veins in human skin.
Study: Video and images of subcutaneous veins were acquired using the rear-facing iSight camera from an iPhone 6, with a fixed aperture of f/2.2, and Sony Exmor RS back-illuminated CMOS image sensor with pixel generation of 1.5 microns. A custom program was written for the iOS operating system that performs a scaled matrix subtraction of different spectral channels and displays results as a grayscale image.
Results: A scaled subtraction of green channel pixel values from red channel pixel values enabled greatly improved identification of subcutaneous veins. Wavelengths of light at which the green detector is most sensitive (520–580 nm) correspond to local absorption maxima of both oxyhemoglobin (542 and 576 nm) and deoxyhemoglobin (556 nm); consequently, the algorithm obtained images of light transport weighted toward deeper skin layers.
Conclusion: We identified and developed a simple algorithm by which a standard smartphone camera can be employed for enhanced video-rate visualization of veins in human skin. Lasers Surg. Med. 50:1034–1039, 2018.

Key words: smartphone; camera; veins; multispectral; imaging

INTRODUCTION

The identification of subcutaneous veins is a critical skill for phlebotomists, nurses, and physicians. Venous access is a preferred means of drawing blood samples for laboratory testing and administering medications or fluid resuscitation in hospitalized patients. Commonly, the subcutaneous veins of the forearm are used as sites of venous access for intravenous line insertion. The inability to rapidly obtain peripheral venous access may lead to delays in the administration of critical medications, or may necessitate the use of more invasive forms of venous access having a higher complication rate, such as central venous catheters. Vein identification is typically accomplished by palpation and visual inspection; however, it may be challenging to identify veins in patients with high BMI, dark skin pigmentation, or small vein caliber.

Human veins appear blue in skin as a result of combined effects from light absorption by hemoglobin and deoxyhemoglobin, wavelength-dependent tissue scattering, blood oxygenation state, vein diameter and depth, and human color perception [1]. In order to facilitate vein visualization, a number of techniques have been proposed. One approach is to place a light source in close contact with the skin. Transillumination using a broadband (white) halogen light source coupled to a C-shaped ring via fiber optic has been shown to improve the rate of first-attempt venous cannulation in a pediatric population (Veinlite, Translite LLC, Sugar Land, TX) [2]. Orange and red LED light sources have also been used for this purpose. Another similar approach uses infrared light to illuminate the skin and generates an image of the infrared reflectance. This approach takes advantage of the increased depth of penetration of infrared light, and its absorption by deoxyhemoglobin in veins. Because the near infrared light is invisible to the naked eye, the vein pattern is then projected onto the skin surface using a visible wavelength, or displayed on a screen [3]. Each of the aforementioned methods requires a dedicated, specialized detection and/or illumination device, which increases the cost and difficulty of implementation. An alternative, multispectral, computational approach to vein imaging using Wiener spectral estimation has been previously successfully demonstrated on a smartphone [4]. We propose a method by which a standard smartphone camera and a comparatively simple algorithm can be employed for the enhanced video-rate visualization of veins in human skin, without prior calibration or the need for additional computational steps

Conflict of Interest Disclosures: All authors have completed and submitted the ICMJE Form for Disclosure of Potential Conflicts of Interest and none were reported.
Contract grant sponsor: ASLMS.
*Correspondence to: Walfre Franco, PhD, Wellman Center for Photomedicine, Massachusetts General Hospital, 50 Blossom St., Boston, MA 02114. E-mail: wfranco@mgh.harvard.edu
Accepted 21 May 2018
Published online 6 June 2018 in Wiley Online Library (wileyonlinelibrary.com).
DOI 10.1002/lsm.22949

such as histogram stretching, as in the aforementioned Wiener spectral estimation method.

MATERIALS AND METHODS

A custom program was written for the iOS system for deployment on an iPhone using the Swift programming language, in which automatic focusing, exposure, and white balance were left enabled. Images were acquired using the rear-facing iSight camera from an iPhone 6. The iSight camera aperture is fixed at f/2.2, and uses a Sony Exmor RS back-illuminated CMOS image sensor with a picture element (pixel) generation of 1.5 microns. In order to obtain an image showing improved contrast of subcutaneous veins, the green and red channels of each image were extracted as spatially co-registered n by n matrices of equivalent dimensions each containing a range of pixel values from 0 to 255. A matrix subtraction was performed in which the value of the green channel is subtracted from the value of the red channel, and resultant pixel values are then displayed equivalently on the red, green, and blue channels of each pixel, yielding a grayscale image in which subcutaneous veins appear dark against a lighter background.

In order to provide quantitative and statistical estimates of enhanced vein visualization, we used pixel intensity values to calculate relative contrast, standard deviations, and entropy. For this purpose, color images were converted to grayscale images following the standard method of forming a weighted sum of the red (R), green (G), and blue (B) components: $0.2989 * \mathrm{R} + 0.5870 * \mathrm{G} + 0.1140 * \mathrm{B}$. Weber contrast is defined as $(I_{\mathrm{min}}–I_{\mathrm{b}})/I_{\mathrm{b}}$, where I_{min} is the minimum intensity value and I_{b} is the background intensity calculated as the average pixel intensity. Michelson contrast is defined as $(I_{\mathrm{max}}–I_{\mathrm{min}})/(I_{\mathrm{max}} + I_{\mathrm{min}})$, where I_{max} is the maximum intensity value. Entropy of the image is defined as $-\Sigma p_{\mathrm{n}} \log_2(p_{\mathrm{n}})$, where n is the number of gray levels and p_{n} is the probability associated with the gray level n.

RESULTS

A scaled subtraction of green channel pixel values from red channel pixel values enabled improved visualization of subcutaneous veins of the upper extremity, as seen in screen images captured from the smartphone application (Fig. 1). Wavelengths of light at which the green detector is most sensitive (520–580 nm) correspond to local absorption maxima of both oxyhemoglobin (542 and 576 nm) and deoxyhemoglobin (556 nm); consequently, the algorithm obtained images of light transport weighted toward deeper skin layers, evidenced by the loss of skin surface textural detail in the scaled images (Fig. 2). Red light was more strongly absorbed by deoxyhemoglobin than oxyhemoglobin by a factor of 10, enhancing contrast of veins in surrounding tissue.

An illustration of the algorithm's application applied after image capture to a standard RGB image is shown in Figure 3. The enhanced vein visualization image (Fig. 3c) reveals the junction of the cephalic and basilic veins, the proximal portion of the median vein of the forearm, and a variety of small tributary veins unseen in the normal (Fig. 3a) or grayscale (Fig. 3b) images.

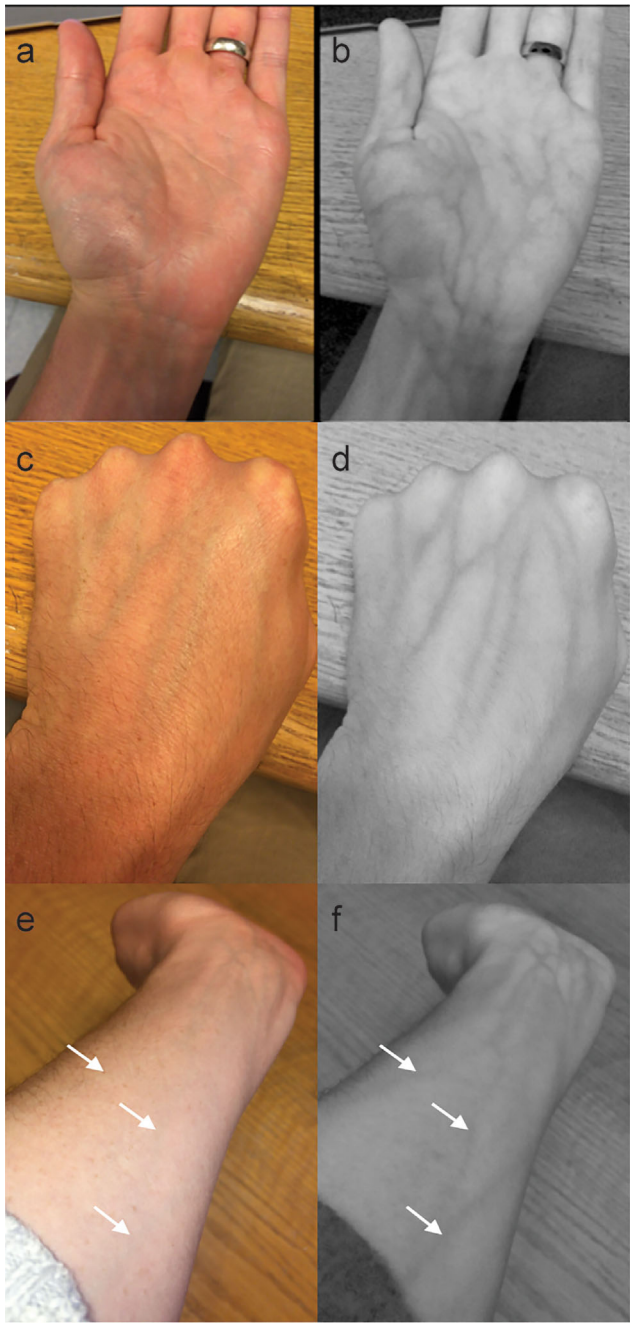

Fig. 1. A scaled subtraction of green channel pixel values from red channel pixel values enabled improved visualization of subcutaneous veins of the upper extremity, as seen in screen images captured from the smartphone application: standard RGB and enhanced visualization images of the (**a**,**b**) palm, (**c**,**d**) back of the hand, and (**e**,**f**) forearm, respectively.

Figure 4 shows pixel intensity values across veins and surrounding tissue without and after applying scaled subtraction of the green channel pixel values to images of the palm. Table 1 shows computations of relative

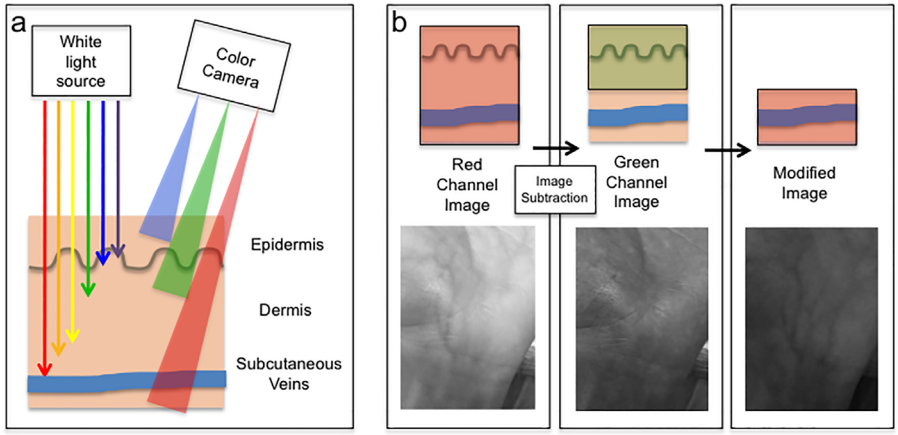

Fig. 2. Wavelengths of light at which the green detector is most sensitive (520–580 nm) correspond to local absorption maxima of both oxyhemoglobin (542 and 576 nm) and deoxyhemoglobin (556 nm); consequently, the algorithm obtained images of light transport weighted toward deeper skin layers, evidenced by the loss of skin surface textural detail in the scaled images. (**a**) Depths of light illumination and camera detection. (**b**) Imaging and subtraction of deep and superficial skin layers.

contrast values and standard deviations of regions of interest on the palm as indicated in Figure 4. Table 2 shows computations of the entropy and standard deviation of the complete images of the palm shown in Figure 4.

DISCUSSION

While multispectral imaging often utilizes dedicated equipment, a normal consumer camera is in fact a multispectral imaging apparatus, operating with three broadband detectors: red, green, and blue. The camera image sensor consists of an array of millions of picture elements (pixels), each with an associated red, green, or blue bandpass optical filter. The red, green, and blue components of an image are detected and recorded on different channels. Using information from these three channels, it is possible to weight an image toward visualization of particular skin chromophores based on their spectroscopic characteristics (which wavelengths of light they absorb) and the transport of light in skin

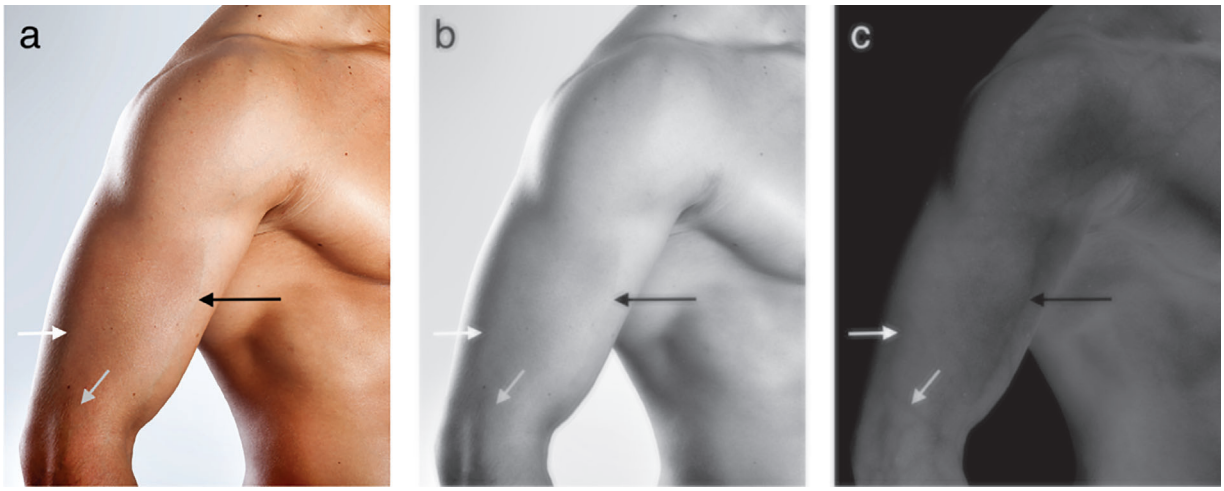

Fig. 3. An illustration of the algorithm's application applied after image capture to an image of skin obtained from the public domain. (**a**) Standard PNG RGB image, with the horizontal white arrow indicating the location of the cephalic vein, the horizontal black arrow indicating the location of the basilic vein, and the oblique gray arrow indicating the location of a vein at the divergence of the basilic and cephalic veins from the median vein of the forearm. (**b**) Grayscale image of the same. (**c**) The image obtained by subtracting the intensity values of the green channel of the image from the intensity values of the red channel of the image and displaying the result as a grayscale image, revealing the junction of the cephalic and basilic veins, the proximal portion of the median vein of the forearm, and a variety of small tributary veins unseen in the normal or grayscale images.

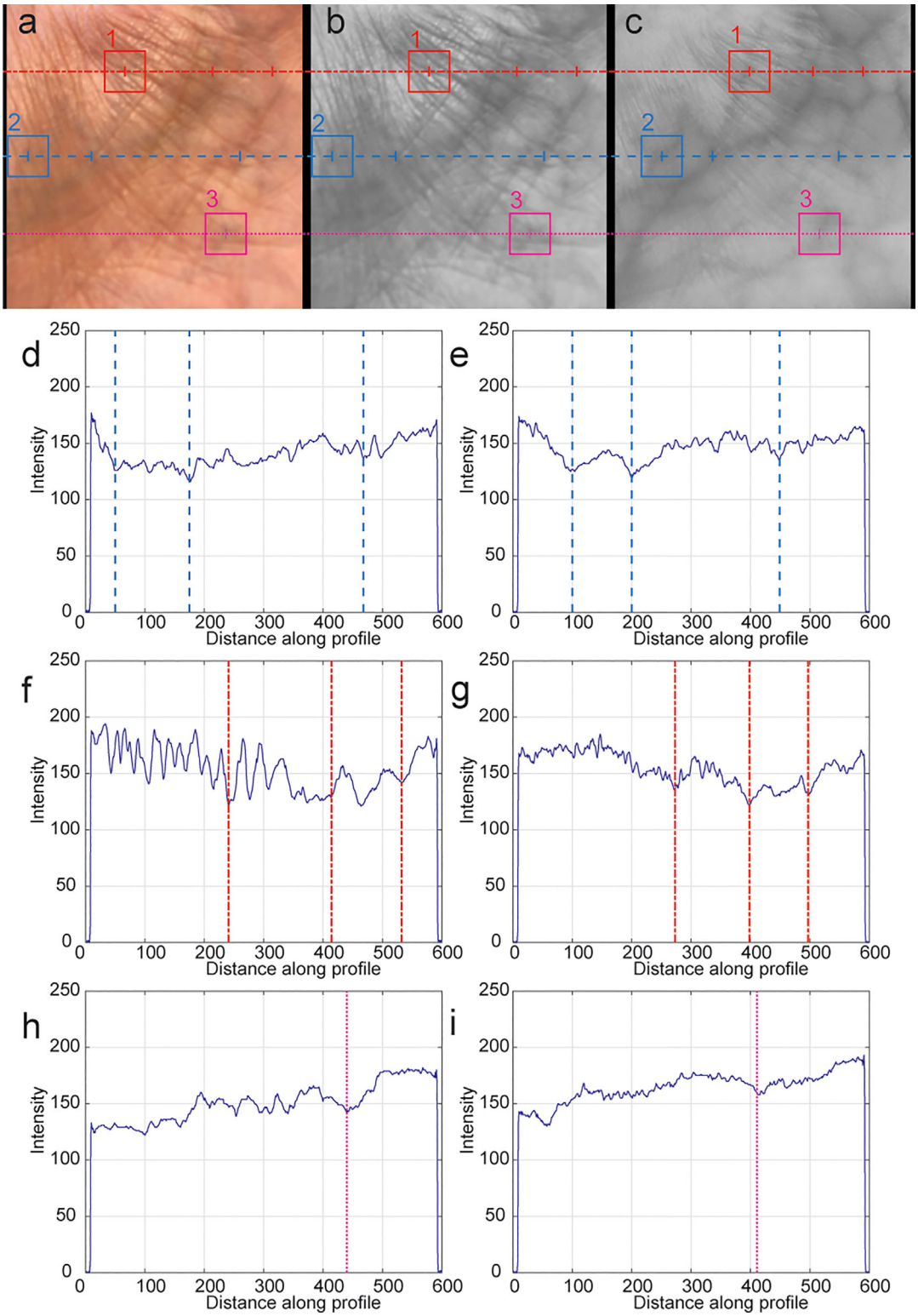

Fig. 4. Profiles of pixel intensity along the lines indicated on (**a**) normal color, (**b**) grayscale, and (**c**) enhanced vein visualization images of the palm. Color and enhanced vein visualization images were obtained with a smartphone in two consecutive shots. The grayscale image was obtained from the color image. The line profiles shown in (**d**), (**f**), and (**h**) correspond to the red, blue, and magenta lines depicted on the grayscale image (**b**), respectively. The line profiles shown in (**e**), (**g**), and (**i**) correspond to the red, blue, and magenta lines depicted on the enhanced vein visualization image (**c**), respectively.

TABLE 1. Weber and Micheslon Contrast Are Respectively Defined as $(I–I_b)/I_b$ and $(I_{max}–I_{min})/(I_{max}+I_{min})$

	Weber contrast		Michelson contrast		Standard deviation	
ROI	Grayscale	Enhanced vein visualization	Grayscale	Enhanced vein visualization	Grayscale	Enhanced vein visualization
1. Red box	−0.22	−0.18	0.28	0.19	16.18	9.29
2. Blue box	−0.14	−0.12	0.19	0.14	11.48	6.68
3. Magenta box	−0.14	−0.15	0.14	0.13	10.61	7.39

(scattering and absorption effects from all skin chromophores).

The reflectance spectrum of skin is well characterized, with the greatest contribution from the red region of the spectrum, and decreased reflectance in the green and blue due to absorption of these wavelengths by melanin and hemoglobin. The red channel of a camera images light that has been scattered through deeper dermal skin structures. Meanwhile, the wavelengths at which the green channel detector is most sensitive (roughly 530–545 nm) correspond to absorption maxima of both oxy- and deoxyhemoglobin; as such, green light has a shallower depth of penetration into skin than red light. By subtracting the brightness values of the green channel from the brightness values of the red channel in an image, one may obtain an image of light transport weighted toward deeper skin layers. Red light is more strongly absorbed by deoxyhemoglobin than oxyhemoglobin, meaning that light transport from the deeper layers of skin will be attenuated over areas where veins are present.

Because of the strong absorption of the blue channel by epidermal melanin in the first 100–200 microns of the skin, the depth of penetration of blue light into the skin is significantly less than that of green or red light, and is less useful for the purpose of imaging deeper subcutaneous veins. However, isolation of images from this channel may prove useful for other similar image processing algorithms, such as highlighting pigmented lesions, or the absence of pigmentation (in vitiligo or ash leaf spots, for instance).

In order to provide quantitative and statistical estimates of enhanced vein visualization, we used pixel intensity values to calculate relative contrast, standard deviations, and entropy of the grayscale and enhanced vein visualization images of a palm (Fig. 4). The normal color image of the palm (Fig. 4a) that contains pixel intensity values from the red, green, and blue detectors was converted to a grayscale image. This grayscale image (Fig. 4b) was used for calculations and comparison to the enhanced vein visualization image (Fig. 4c) of the same palm. Figure 4 shows line profiles of pixel intensity values of the grayscale and enhanced vein visualization images. Because of the increased absorption of blood in veins relative to the surrounding tissue, the location of a vein should correspond to a valley or local minimum in the line profiles intensity of pixel intensity. This is illustrated in Figure 4 where the horizontal lines in the line profiles indicate the local minimum in signal that corresponds to vein location in the images of the palm. Figure 4 also illustrates that local minima are easier to identify in the enhanced vein visualization images, Figure 4e, g, and i. This signal feature is also present in Figure 4d, f, and h, however, it is embedded in noise generated by combining signals from the red, blue, and green detectors. Relative contrast values and standard deviations of intensity computed for the regions of interest (ROI) depicted in Figure 4b and c are shown in Table 1. Note that there is more contrast and the standard deviation is larger in the grayscale image ROIs. The improvement in vein visualization is not necessarily higher contrast but rather removing unnecessary information. The standard deviation of the ROIs indicates a reduced dispersion in intensity values of the enhanced vein visualization images. The global standard deviation and entropy of the complete enhanced vein visualization image are also lower, Table 2. Entropy is a statistical measure of randomness or the amount of disorder in a system, or the spread of states which a system can adopt. For an image, the states correspond to the gray levels that a pixel can have, for example, in an 8-bit pixel image there are 256 states. Lower entropy in an image implies that less states are occupied and less information content. In our case, reduced noise and the appropriate information content.

TABLE 2. Entropy and Standard Deviation of the Grayscale and Enhanced Vein Visualization Images Shin in Figure Y

	Grayscale	Enhanced vein visualization
Entropy	6.32	6.05
Standard deviation	31.03	29.62

Entropy is defined as $-\Sigma p_n log_2(p_n)$ where n is the number of gray levels and p_n is the probability associated with gray level n. Standard deviation of the pixel intensity values.

CONCLUSION

In conclusion, we have demonstrated a simple algorithm by which a smartphone camera may be used to produce enhanced real-time images of subcutaneous veins. The basic principle at work may be extended to other situations in which imaging of particular skin chromophores at a target depth is desired. Further work to understand the

performance of the algorithm in a range of clinical subjects of varying anatomy, skin pigmentation, and BMI will be necessary in order to fully characterize the algorithm's performance and appropriateness for use in various clinical settings. Of note, the source of illumination in a typical clinical setting is typically broadband, but will vary based on whether illumination is accomplished by sunlight, mercury fluorescent lamp, incandescent lamp, LED lamp, or flash. In our experience, this did not significantly alter the utility of the algorithm, though specular reflection or glare can limit the technique's performance.

ACKNOWLEDGMENTS

We gratefully acknowledge the support of ASLMS in providing a travel grant to allow for presentation of this work at the ASLMS 2017 annual conference. The authors gratefully acknowledge the support of Dr. R. Rox Anderson.

REFERENCES

1. Kienle A, Lilge L, Vitkin IA, et al. Why do veins appear blue? A new look at an old question. Appl Opt 1996;35:1151.
2. Katsogridakis YL, Seshadri R, Sullivan C, Waltzman ML. Veinlite transillumination in the pediatric emergency department: A therapeutic interventional trial. Pediatr Emerg Care 2008;24:83–88.
3. de Graaff JC, Cuper NJ, Mungra RA, et al. Near-infrared light to aid peripheral intravenous cannulation in children: A cluster randomised clinical trial of three devices. Anaesthesia 2013;68:835–845.
4. Chen S, Liu Q. Modified Wiener estimation of diffuse reflectance spectra from RGB values by the synthesis of new colors for tissue measurements. J Biomed Opt 2012; 17:030501.